

Kitchen-grade aluminium foil as dual-purpose substrate-cum-electrode for ultrathin, ultralight, and bendable perovskite solar cells

Arun Kumar^{a,b,*}, Sonia Rani^{a,b}, Dhriti Sundar Ghosh^{a,b,**}

^a Thin-film and Photovoltaics Laboratory, Department of Physics, Indian Institute of Technology Dharwad, Dharwad, India

^b Department of Physics, Indian Institute of Technology Bhilai, Raipur, India



ARTICLE INFO

Keywords:

Metal foil
Lightweight
Flexible
Perovskite solar cell
Oxide-metal-oxide

ABSTRACT

Flexible and lightweight photovoltaics have attracted great attention in recent years owing to their application in wearable and portable electronic devices. However, the use of polymer substrates obstructs the fabrication of highly efficient and stable devices due to their limitations like low transmittance, poor temperature tolerance, photodegradation, high material cost, etc. In addition, conventional flexible transparent electrodes (TEs) such as indium tin oxide (ITO) deposited on polymeric substrates have poor electro-optical properties compared to their glass counterpart and are still brittle, which not only negatively affect the performance but also the flexibility/bendability. Here in this work, a kitchen-grade aluminium foil providing a lightweight, low-cost, mechanically flexible substrate-cum-electrode has been utilized for the very first time in the fabrication of perovskite solar cells. Also, an indium-free, oxide-metal-oxide (OMO) based TE exhibiting a sheet resistance below $6 \Omega/\square$ and an average visible transmittance above 80% is used as a top TE. A power conversion efficiency (PCE) of over 10% is obtained with a high power per unit weight of over 3.5 W/g, which is much higher than conventional solar cells. The present work traces a way towards the fabrication of lightweight and flexible photovoltaic/optoelectronic devices by incorporation of metallic foil as substrate-cum-electrode.

1. Introduction

The continuously growing global energy demand has driven the urgent need to transition from fossil fuels to renewable energy sources. In this regard, solar energy stands out as a viable and abundant alternative. The Sun's irradiation on the Earth's surface in just 1 h surpasses the total annual global energy demand. Harnessing even a small fraction of this solar energy resource has the potential to fulfil the escalating energy needs of our planet. To facilitate the widespread adoption of solar power and make it more efficient and accessible, there is a compelling requirement for photovoltaic technology that is both cost-effective and highly efficient. With the rising popularity of wearable electronic devices and electric vehicles, it has become crucial to develop solar cells that seamlessly integrate with these devices without compromising their aesthetics or adding unnecessary weight.

Bendable and lightweight solar cells offer an innovative solution to these challenges. Their bendable characteristics allow them to conform to the desired shape of the target device or vehicle, enabling seamless integration and preserving the overall design aesthetics. Additionally,

the use of thin substrates, photoactive layers, and other functional layers in these cells not only enhances their flexibility but also ensures they remain lightweight, making them an ideal choice for low-weight additions to various applications [1–4]. Among the emerging energy harvesting technologies, perovskite solar cells (PvSCs) have gained considerable attention due to their remarkable power conversion efficiency (PCE) and comparatively lower production costs [5,6]. The unique properties of perovskite materials enable them to exhibit a high absorption coefficient, meaning they can absorb incident sunlight using a thinner layer of photoactive material compared to conventional solar technologies. This property holds tremendous potential for the development of flexible/bendable and lightweight solar cells, as it allows for efficient light absorption and utilization while maintaining the required structural flexibility. When it comes to fabricating flexible and lightweight solar cells, conventional choices for substrates have included indium tin oxide (ITO) coated Polyethylene naphthalate (PEN) or Polyethylene terephthalate (PET). While these polymer substrates offer flexibility, they suffer from lower stability when exposed to ultraviolet (UV) light [7,8]. Prolonged exposure to sunlight can cause these

* Corresponding author. Thin-film and Photovoltaics Laboratory, Department of Physics, Indian Institute of Technology Dharwad, Dharwad, India.

** Corresponding author. Thin-film and Photovoltaics Laboratory, Department of Physics, Indian Institute of Technology Dharwad, Dharwad, India.

E-mail addresses: 222083001@iitdh.ac.in (A. Kumar), dhriti.ghosh@iitdh.ac.in (D. Sundar Ghosh).

substrates to fade, leading to reduced transmittance and subsequently impacting the illumination of the photoactive layer, thereby decreasing overall device performance. Furthermore, the use of thick ITO film as a transparent electrode (TE), despite providing good conductivity and transmittance, presents its own challenges. ITO films are inherently brittle, limiting their ability to withstand successive bending cycles when employed in flexible optoelectronic devices. As a result, the performance of these devices tends to degrade over time. Additionally, the rarity of indium, a key component of ITO, contributes to its high cost, further increasing the overall device expense [2,9,10].

To overcome these limitations, in this work a novel approach has been proposed and evidenced. We have demonstrated a lightweight and bendable PvSC utilizing an inexpensive and readily available kitchen-grade aluminium foil (Al-foil) serving as a dual purpose of a substrate and an electrode. Being a metal foil, it offers numerous advantages for device applications. They provide a pathway with low resistance for charges to flow, enhancing device performance by reducing series resistance. Additionally, they are lightweight, cost-effective, and can be easily shaped to suit different needs. However, the presence of high surface roughness in kitchen-grade Al foil poses major challenges. The rough surface can lead to issues like poor contact, uneven current distribution, and weak adhesion. These factors can undermine device functionality and reliability. To overcome these challenges, various techniques can be employed. For example, smoothing the surface through polishing or chemical etching helps improve uniformity. Applying protective or conductive coatings can also mitigate the impact of roughness and enhances contact properties. By addressing these challenges, the advantages of metal foils, such as their low resistance, lightweight nature, and cost-effectiveness, can be fully utilized, resulting in improved device performance and functionality. Nonetheless, the surface roughness issue can also be eliminated by simply choosing a smoother but costlier metal foil as demonstrated earlier.

To enhance the surface properties of the rougher Al foil used in this work, a relatively thick layer (~ 300 nm) of titanium (Ti) is deposited onto it, creating a smoother surface that is more suitable for subsequent device layers. The Ti layer is further partially thermally oxidized leading to the conversion of the top portion of the film into titanium dioxide (TiO_2), which apart from surface smoothening also acts as an electron transport layer (ETL) without requiring the deposition of additional ETL materials in the device. The photoactive layer, $\text{CH}_3\text{NH}_3\text{PbI}_3$, is then deposited on top of the TiO_2 layer, followed by the deposition of spiro-OMeTAD as a hole transport layer (HTL). To serve as the top TE, an oxide-metal-oxide (OMO) stack is employed. This choice is driven by the OMO stack's desirable properties, including high conductivity, high transmittance, and excellent resistance to degradation when subjected to bending or flexing. Compared to traditional transparent conductive oxides (TCOs), the OMO stack exhibits superior mechanical robustness, ensuring the longevity and reliability of flexible and lightweight solar cells [11,12]. The optimization of the top TE is achieved through the utilization of advanced optical modeling techniques, which aid in fine-tuning the electrode structure to maximize performance by minimizing the residual reflection and hence improving the overall transmittance.

Through this innovative approach, we have fabricated and demonstrated bendable and lightweight PvSCs have achieved a notable PCE of 10.64% along with an impressive power-to-weight ratio of over 3.5 W/g. Furthermore, these solar cells demonstrate a T_{80} lifetime of 500 h in ambient atmospheric conditions, even without the need for additional encapsulation. This achievement showcases the immense potential of the proposed method for producing efficient, durable, and cost-effective bendable and lightweight solar cells that can be seamlessly integrated into various applications, including wearable electronic devices and electric vehicles. By harnessing the power of perovskite materials and leveraging the advantages of Al-foil as a substrate-cum-electrode, this work represents a significant step forward in the advancement of renewable energy technologies, offering a promising solution to meet

the ever-increasing energy demands of our modern world.

2. Experimental section

2.1. Fabrication

In the fabrication process, a commercially available kitchen-grade Al-foil (Fig. S1) was chosen as the substrate-cum-electrode for fabricating planar PvSC. The Al-foil had a thickness of ~ 11 μm . To prepare the foil for the subsequent steps, it underwent thorough cleaning by rinsing it with deionized (DI) water and isopropyl alcohol (IPA). This cleaning process ensured the removal of any impurities or contaminants that could affect the performance of the solar cells. After the cleaning step, the Al-foil was subjected to argon plasma treatment. This treatment further improved the cleanliness of the substrate, promoting better adhesion and uniformity in the subsequent layers. To overcome the high surface roughness of the Al-foil and achieve a smooth and planar surface, a thick layer of Ti was deposited on the plasma-treated Al-foil. The titanium layer served as a planarization layer, helping to create a more uniform surface for the subsequent layers of the solar cell. The deposition of the Ti layer was carried out using DC magnetron sputtering. Moorfield nano_PVD S10A system was used for the deposition. High-purity Ti with a diameter of 2 inches was used as the target material. The sputtering chamber was evacuated to a vacuum level better than 5×10^{-7} mbar. During the Ti deposition, a working pressure of 3×10^{-3} mbar and a power of 100 W were maintained. These parameters were optimized to achieve the desired thickness and quality of the Ti layer. Following the Ti film deposition, the substrates were subjected to annealing treatment. In this case, the annealing step aimed to oxidize the top part of the Ti film into titanium dioxide (TiO_2). The conversion of Ti to TiO_2 is significant because TiO_2 can itself function as an ETL without the need for an additional ETL deposition. The annealing process involved heating the substrates to a temperature of 500 °C for 30 min, followed by a cooling period. Due to the higher thickness of the Ti layer only partial oxidation of the layer takes place, which leads to a bilayer structure of Ti (bottom) and TiO_2 (top) which we will collectively call as Ti_Oxd in this manuscript from now onwards. After the annealing step, the substrates were cleaned again using low-power argon plasma. This cleaning process was carried out carefully at low power and pressure to avoid etching of the TiO_2 layer. The cleaned substrates were then transferred to a nitrogen-filled glove box. In the glove box, the active layer of the solar cell was deposited on the Al-foil/Ti_Oxd substrates using a one-step spin-coating method. The precursor solution for the active layer was prepared by mixing lead iodide (PbI_2), methylammonium iodide (MAI), dimethyl sulfoxide (DMSO), and N,N-dimethylformamide (DMF). 461 mg PbI_2 , 159 mg MAI, 71 μL DMSO, and 640 μL DMF were mixed together [13,14]. The precursor solution was stirred for an hour to ensure a homogeneous mixture. The spin-coating process involved applying the precursor solution onto the substrates and then spinning them at 4000 RPM for 30 s. To enhance the crystallization, 100 μL chlorobenzene as an anti-solvent, was dropped onto the spinning substrates during the last 10 s of rotation. Once the rotation stopped, the substrates were transferred to a preheated hotplate maintained at a temperature of 60 °C. The substrates remained on the hotplate for 1 min, promoting the drying and crystallization of the active layer. Subsequently, the substrates underwent annealing at a temperature of 100 °C for 3 min. These annealing steps were crucial for the formation of the desired black perovskite phase, which is essential for efficient photovoltaic performance. After this, an HTL of spiro-OMeTAD was deposited onto the perovskite layer using spin coating. The spiro-OMeTAD solution was prepared by dissolving 72 mg spiro-OMeTAD in 1 ml chlorobenzene. 28.8 μL *tert*-butyl pyridine and 17.5 μL lithium salt solution (520 mg LiTFSI in 1 ml acetonitrile), were added to enhance the hole transport properties of the HTL. The spin-coating process involved spinning the prepared spiro-OMeTAD solution onto the substrates at 3000 RPM for 30 s [15]. After the

deposition of spiro-OMeTAD, the substrates were taken out of the glove box and kept covered in an ambient environment overnight. To finalize the device fabrication, a top transparent electrode (TE) was deposited over the spiro-OMeTAD layer. The TE consisted of an ultrathin silver (Ag) film sandwiched between nickel oxide (NiO) films. The deposition of the TE was carried out using physical vapor deposition techniques, which involved a combination of thermal and e-beam evaporation. The deposition of the three layers of the NiO/Ag/NiO (NAN) stack was performed sequentially without breaking the vacuum to avoid the oxidation of ultrathin metal film [16]. To further enhance the transmittance of the TE, an additional antireflection coating (ARC) of magnesium fluoride (MgF_2) having a thickness of 40 nm was applied over the NAN-TE using e-beam evaporation. This additional coating aimed to minimize the reflection of incident light from the device surface, thereby increasing the amount of light entering the photoactive layer. Finally, a device with architecture Al-foil/Ti_{Oxd}/MAPI/Spiro-OMeTAD/NAN/MgF₂ has been fabricated as shown in Fig. 1. To the best of our knowledge, this is the first work reporting a PvSC utilizing a kitchen-grade Al-foil as substrate-cum-electrode. The fabricated device comes among the highly efficient devices that utilize a metallic foil both as a substrate and electrode exhibiting a PCE of 10.64%. Apart from this, it is also one of the cheapest, thinnest and lightest (power/weight ~ 3.5 W/g) PvSC incorporating a metallic foil substrate. For comparison, a list of PvSCs fabricated on metallic foils previously reported has been tabulated in the supplementary information (Table S1) [17–22].

2.2. Characterizations

Various characterizations were conducted to optimize, evaluate, and analyze the properties and performance of different layers and fabricated devices. Optical characterizations, such as transmittance and reflectance measurements, were performed on the top and bottom electrodes. The Shimadzu UV-2600 ISR UV–Vis spectrophotometer was used for these measurements. Reflectance measurements were conducted on the Ti-coated Al-foil before and after the annealing process to confirm the oxidation of the Ti layer, a critical step in TiO₂ ETL formation. Transmittance spectra were studied for the NAN-TE with and without the MgF₂ coating to gain insights into the light entering the device. The surface roughness of the Al-foil, both with and without the Ti_{Oxd} layer, was measured using atomic force microscopy (AFM) images obtained from the Bruker Dimension Icon. This analysis provided information about surface morphology and the impact of the Ti_{Oxd} layer on substrate roughness. To analyze the work function of the fabricated top NAN-TE, Kelvin probe force microscopy (KPFM) analysis was conducted using a platinum-iridium-coated conductive tip to figure out the work function, which indicates the compatibility of the NAN-TE as a hole collector electrode. For structural studies, X-ray diffraction (XRD) analysis was performed using a D8 Advance XRD instrument. The analysis was carried out in a grazing incidence XRD (GIXRD) configuration, with a fixed incident angle of 0.5° and varying 2θ angles from 30° to 90° and 10°–60° for Ti_{Oxd} and perovskite layer respectively, which confirms the oxidation of Ti film and phase composition of the fabricated

perovskite layer. To examine the surface morphology of the fabricated photoactive perovskite layer on the Ti_{Oxd}-coated Al-foil, field emission scanning electron microscopy (FESEM) was conducted. FESEM images were captured using a Carl Zeiss Gemini SEM 500 instrument with a magnification of 100,000× that provides the opportunity for the visualization of the surface morphology and the assessment of the perovskite layer's uniformity and quality. To evaluate the photovoltaic behaviour of the fabricated devices, current density-voltage (JV) measurements were performed using an Enlitech SS-F5 class AAA Solar simulator in conjunction with a Keithley source meter 2450. The active area of the device was illuminated with 1 Sun (AM 1.5G) light, and an aperture size of 0.0625 cm² was used for the measurements. Additionally, the spectral response of the devices was analyzed using external quantum efficiency (EQE) measurements. An Enlitech QE-R instrument, equipped with a power source (75 W xenon lamp), a monochromator, and a light chopping mechanism, was employed for the EQE measurements. The spectral range analyzed was from 300 nm to 900 nm. For stability analysis, the fabricated devices were exposed to ambient atmosphere conditions with 35–45% relative humidity and temperature 25–40 °C for 500 h without any encapsulation. JV characteristics were periodically measured during this duration to monitor the stability and performance degradation of the devices over time. For flexibility analysis, the device was pasted on a PET substrate providing a firm support to the Al-foil. Flexibility tests were performed using an L-shaped two-point bend testing mechanism attached to a motor allowing the arm to move back and forth along the horizontal axis as reported elsewhere [23]. Correspondingly, the solar cell was bent up to a 5 mm radius of curvature. The bending analysis provides information regarding the mechanical robustness of the devices.

3. Results and discussion

To proceed with the experimental realization of the device, we opted to utilize a kitchen-grade Al-foil due to its wide availability and low cost. As mentioned above, the Al-foil while possessing a surface that is unpolished and rough, poses certain challenges [21]. The high roughness of the foil could adversely affect the deposition of subsequent layers, consequently impacting device performance. Additionally, the rough surface could provide more shunting paths, resulting in increased carrier recombination and decreased device performance [24]. To evaluate the surface roughness, we employed AFM and found that the bare Al-foil exhibited a relatively high RMS roughness of around 9.3 nm as shown in Fig. 2(a). To address the roughness issue, we implemented a strategy involving the deposition of a thick layer (300 nm) of Ti onto the Al-foil using DC magnetron sputtering. Subsequently, we subjected the deposited Ti film to thermal annealing, which induced oxidation of the top portion, transforming it into a TiO₂ layer.

To optimize the performance of device stacks with varying thicknesses of Ti and TiO₂, we conducted a comprehensive study using optical modelling utilizing the transfer matrix method (TMM) [25,26]. By systematically adjusting the thicknesses of Ti and TiO₂ in the device stack, we aimed to understand the impact of these variations on the device

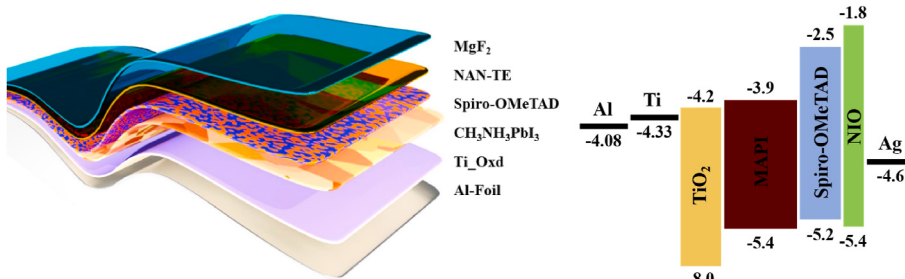


Fig. 1. The schematic architecture of the photovoltaic device fabricated on a kitchen-grade Al-foil and energy band diagram of the same.

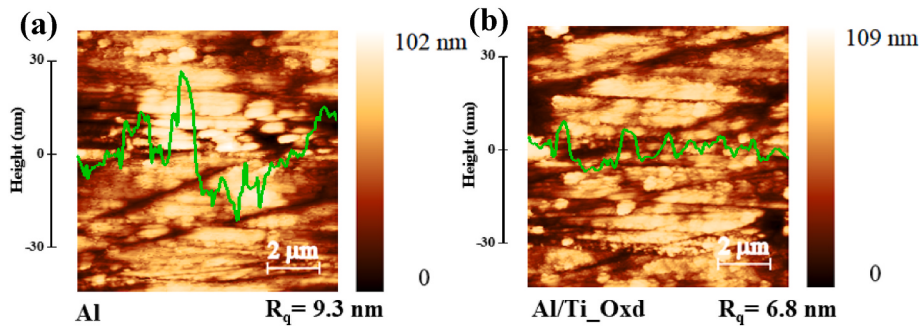


Fig. 2. AFM images revealing surface morphology of (a) bare Al-foil and (b) thermally oxidized Ti coated Al-foil over an area of $10 \mu\text{m} \times 10 \mu\text{m}$. R_q represents the RMS value of the surface roughness. The green line in both figures is showing the cross-section profilometry.

performance. Surprisingly, our observations revealed that the device performance remained relatively unaffected by the thickness variations (Figs. S2 and S3). We found that different Ti and TiO_2 thicknesses combinations within partially oxidized 300 nm Ti film, yielded comparable device performance. Based on these findings, we adopted a low-cost fabrication approach by annealing the Ti film under ambient air conditions, without stringent control over oxygen and pressure conditions. This method ensured an efficient and cost-effective fabrication route for our devices. This annealing step resulted in the formation of Ti_{Oxd} layer which served a dual purpose, acting as a planarization layer and an ETL, simultaneously [27]. The AFM analysis revealed a notable decrease in RMS surface roughness to around 6.8 nm upon the formation of Ti_{Oxd} as seen in Fig. 2(b). Moreover, the transformation of the top surface from a conductive metal (Ti) to an ETL (TiO_2) mitigated the risks associated with carrier recombinations through shunting paths. Furthermore, this modification provided an improved platform for the adhesion and deposition of subsequent layers.

We also investigate the impact of thermal annealing on the reflection spectra of Ti-coated Al-foil. Before the annealing process, the spectra showed a significant reflection, which decreased after thermal annealing. This reduction in reflection observed in Fig. 3(a) can be attributed to the partial oxidation of the Ti film, leading to the formation of TiO_2 .

To ensure the partial conversion of Ti film to TiO_2 , we performed a GIXRD analysis for Ti_{Oxd} . When analyzing the XRD spectra before and after annealing the deposited Ti film, a shift in some of the peaks has been observed, which confirms the presence of both Ti and TiO_2 phases in the Ti_{Oxd} film, and the same can be seen in Fig. 3 (b) [28,29]. Again, a similar analysis was performed on the photoactive MAPI layer to confirm the formation of the perovskite phase. The analysis was performed in a 2θ range varying from 10° to 60° . Fig. 4(a) confirms the successful formation of the perovskite phase. The sharp peaks corresponding to MAPI in the XRD pattern indicated its potential for photovoltaic application [30]. The grain size and boundaries within the photoactive layer hold profound significance for the performance of

devices. It is widely acknowledged that smaller grains bring an abundance of grain boundaries, resulting in high charge carrier recombination while concurrently reducing charge collection in the devices. Conversely, it has been observed that excessively large grain sizes can give rise to increased surface roughness and the formation of pinholes within the photoactive layer owing to inadequate packing. These detrimental effects lead to elevated series resistance and diminished shunt resistance, consequently reducing the overall efficiency of the device. To assess the surface morphology of the photoactive MAPI film, we employed FESEM. The images obtained in Fig. 4(b) revealed a uniform distribution of grains throughout the film, without any significant pinholes. Individual grain sizes were observed to range between 200 and 300 nm. The presence of such appropriate grain size, along with their uniform distribution and minimal pinhole formation, predicts the achievement of highly efficient devices, as these factors contribute to improved charge transport and reduced recombination losses [31–33].

The illumination of the photoactive layer in the fabricated device presents a challenge due to the inherent light-blocking nature of metallic foil. To overcome this limitation, a highly transparent top-TE contact is necessary. In this study, we utilized a NAN-TE as mentioned in the previous section to resolve this issue. A detailed description of NAN-TE with its optimization, fabrication and integration with the device can be found elsewhere [16,34]. Our investigations into the transmittance of NAN-TE revealed an impressive average visible transmittance (AVT) of over 80%. To further enhance light transmission, we implemented an additional layer of MgF_2 as an ARC, which resulted in an enhancement of around 2.91% in AVT (Fig. 5) more precisely, the transmittance in higher wavelength region increases by ~7%. This improvement in transmittance holds the potential for improving the exposure of the photoactive layer to incident light, consequently boosting photocurrent generation and overall device performance. Additionally, this NAN-TE exhibits a high work function of $\sim 5.35 \text{ eV}$ which makes it compatible as a hole collector [35]. The KPFM image and potential plot can be seen in Fig. S4 (c) of supplementary information.

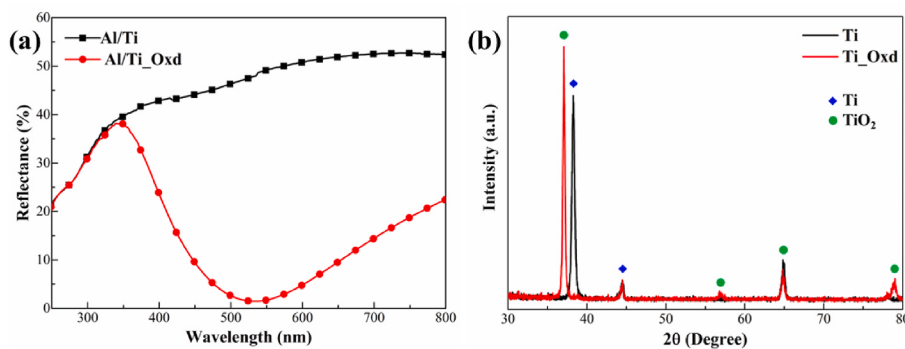


Fig. 3. (a) Reflectance spectra of Ti film before (black) and after (red) annealing at 500°C confirming the oxidation in the Ti metal layer and (b) GIXRD plot of Ti film before (black) and after (red) annealing at 500°C confirming the transformation of Ti to TiO_2 .

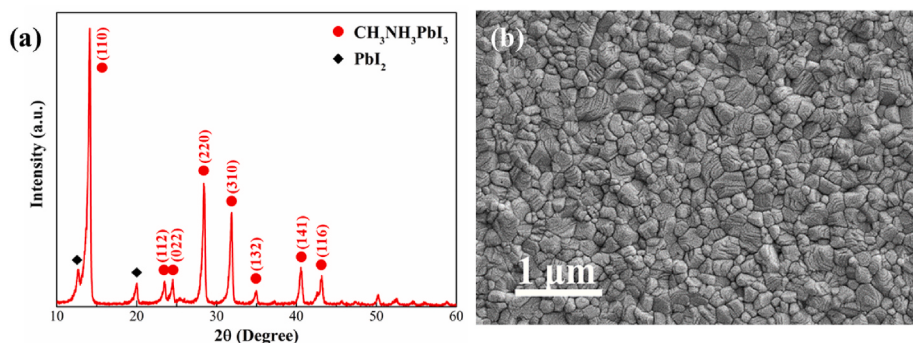


Fig. 4. (a) GIXRD plot of photoactive $\text{CH}_3\text{NH}_3\text{PbI}_3$ layer deposited over Ti_Oxd coated Al-foil revealing sharp peaks corresponding to perovskite phase of the absorber layer and (b) Surface morphology of photoactive layer deposited over Ti_Oxd coated Al-foil suggesting uniform grain distribution throughout the film. The scale in the FESEM image is 1 μm .

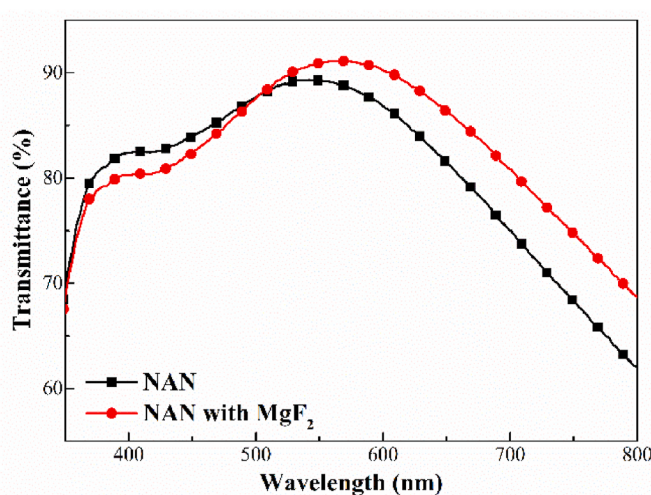


Fig. 5. Transmittance spectra of NAN-TE with (red) and without (black) implementation of MgF_2 ARC obtained from UV-vis spectrophotometer in a wavelength range corresponding to perovskite absorption range.

Once the different device layers have been optimized for their respective role, an integration of all these layers is carried out and an architecture of Al-foil/Ti_Oxd/MAPI/Spiro-OMeTAD/NAN/MgF₂ has been chosen for the device fabrication. However, prior to that, we also checked the functionality of the Ti_Oxd layer as an ETL in the device and compared it.

with conventional SnO₂ on a rigid glass substrate and the same can be found in Figs. S4 and S5. After confirmation of the Ti_Oxd layer as an ETL on a rigid substrate, the actual intended device on Al foil was

realized. By fabricating the device over Al-foil substrate a PCE of 10.64% along with a high power-to-weight ratio of over 3.5 W/g. The device possesses a high J_{SC} value of 20.18 mA/cm^2 along with a V_{OC} of 0.821 V and FF of 64.19%. The photovoltaic performance of the fabricated devices on Al foil with and without integration of MgF_2 ARC have been studied and are shown in Fig. 6(a) and the corresponding electrical parameters are given in Table 1. The findings unveiled a notable improvement in the PCE of the photovoltaic device through the implementation of the ARC. This substantial enhancement primarily originated from an increase in the J_{SC} , resulting from enhanced charge carrier generation. The reason behind this enhancement lies in the improved exposure of the photoactive layer, facilitated by the improved transmittance of the NAN top-TE, by the incorporation of the MgF_2 ARC (Fig. 5) as discussed earlier. For verifying the same, the reflection spectra of the entire device with and without MgF_2 layer has been taken which shows a significant reduction in the device's reflection in higher wavelength region (Fig. 7(a)) and the corresponding increment in the photon flux entering the device can be seen in Fig. 7(b). This shows that more light is entering the device resulting in better illumination of the photoactive layer and hence an improvement in J_{SC} values. Devices with Ti_Oxd thickness of 150 nm and 500 nm were also prepared, however, the device's performance was relatively lower than the 300 nm one due to poor charge collection as discussed in supplementary information and corresponding variation in V_{OC} , J_{SC} , and FF of the device (Fig. S6 (a) and Table S2). Apart from this, different thicknesses on bottom NiO in NAN-

Table 1
Photovoltaic parameters of fabricated devices with and without MgF_2 coating.

Device Parameters	V_{OC} (V)	J_{SC} (mA/cm^2)	FF (%)	PCE (%)
Without MgF_2	0.813	16.96	62.49	8.62
With MgF_2	0.821	20.18	64.19	10.64

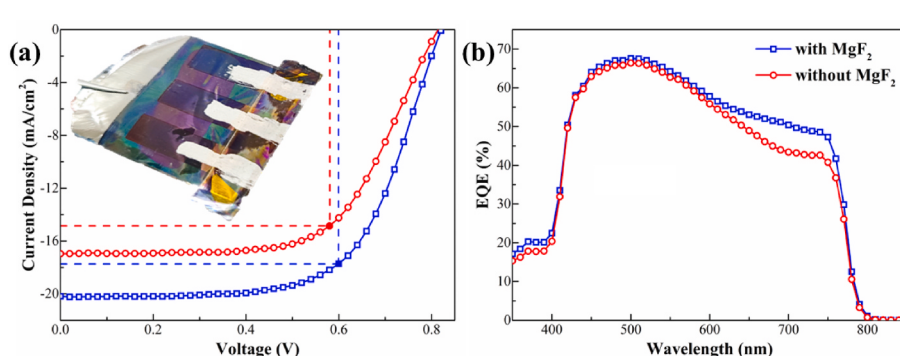


Fig. 6. (a) Current Density-Voltage characteristics and (b) EQE spectra of the fabricated photovoltaic device with (blue) and without (red) MgF_2 ARC, inset (a): A real-time image of the PvSC device fabricated on an Al-foil substrate.

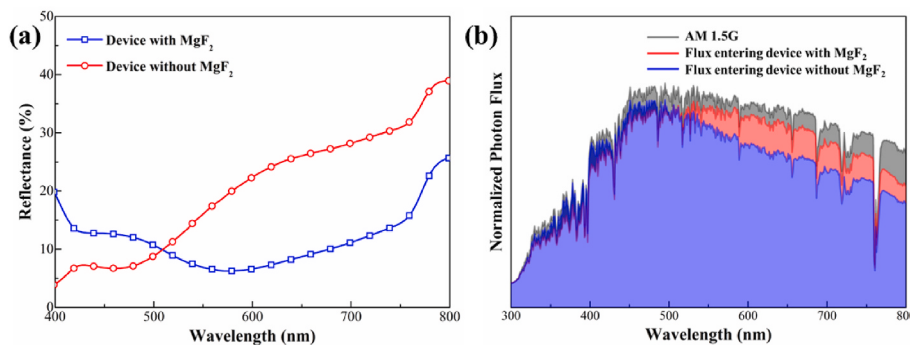


Fig. 7. (a) Reflection Spectra of the complete device with and without MgF₂ indicating light getting reflected from the device when illuminated from the top, (b) Photon flux entering the device with and without implementation of MgF₂ ARC.

TE also have been investigated for device compatibility, and the variation made by the same is explained and can be seen in Fig. S6 (b) and Table S3. By undertaking such optimizations, an impressive PCE of 10.64% was attained, coupled with a specific power (power-to-weight ratio) exceeding 3.5 W/g, positioning it as one of the lightest photovoltaic devices available. To further analyze the spectral response of the fabricated device towards incident light, the EQE spectra were examined, comparing devices with and without the MgF₂ coating. The EQE spectra serve as a valuable source of information about charge carrier generation and transfer within the device. Upon investigating the EQE spectra given in Fig. 6(b), fascinating insights emerged. As the light is entering from the *p*-side, below a wavelength of 400 nm, the spectral response exhibited poor sensitivity, attributed to parasitic absorption within the spiro-OMeTAD layer. Furthermore, on the higher wavelength side, a lower EQE was observed, indicating a higher occurrence of recombination on the back contact side. This phenomenon could be ascribed to inadequate connections and charge leakage at the Ti_Ox layer or metal foil, resulting from high surface roughness and improper interlayer connections. However, the implementation of the MgF₂ layer was found to enhance photogeneration, particularly in the higher wavelength regions. This enhancement was attributed to the improved illumination of the photoactive layer, ultimately leading to EQE values of a maximum value of up to 70% and showcasing a commendable spectral response. This enhancement in EQE in higher wavelength region is in agreement with improved transmittance of NAN-TE by incorporation of MgF₂ ARC and that of reduced reflection losses as discussed earlier, which also confirms the better exposure of photoactive layer and corresponding enhancement in EQE of the device.

To further analyze the compatibility of the demonstrated methodology with upscaling, we fabricated a single-pixel large-area device with an active area of 2 cm² and a PCE of 5.93% was obtained from the same. The decrease in the performance while shifting to a larger area is associated with increased series resistance along with increased shunting paths giving rise to higher probability of recombination and hence decreased performance [36]. The photovoltaic behaviour of the large-area device is shown in Fig. 8.

When it comes to large-scale fabrication and commercialization of PvSCs, stability emerges as a critical factor. The instability of PvSCs primarily occurs from the photoactive perovskite material itself and its interfacial interactions with the adjacent layers. In this study, we investigated the variation in the electrical parameters of the device and the stability exhibited by the fabricated PvSCs has been analyzed. To assess stability, the fabricated devices were subjected to ambient air conditions, characterized by relative humidity of approximately 50% and temperatures ranging from 25 °C to 40 °C, without any encapsulation. As expected, over time, the performance of the devices started to exhibit a decline, a common occurrence in the PvSCs. However, if we go into further detail, it can be seen that V_{OC} of the device slightly increases over the period of time, which might be due to improvement in the

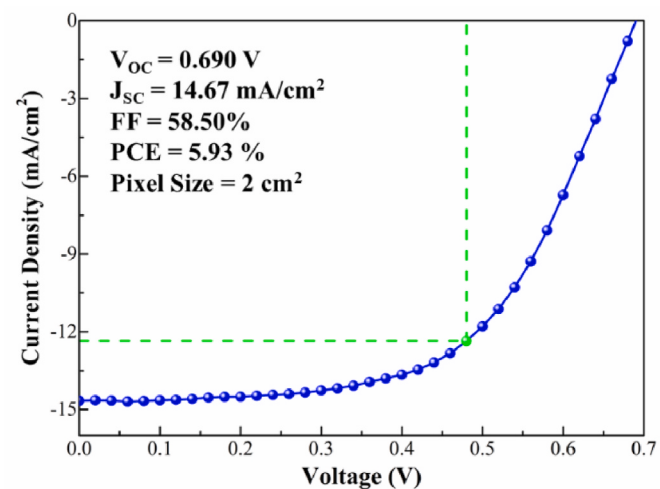


Fig. 8. JV characteristics of the large area (2 cm²) device fabricated on Al-foil. The green sphere represents the maximum power point. **Inset:** electrical parameters of the fabricated large-area device.

morphology of the photoactive layer as reported previously. A continuous decrease in the FF of the device has been observed which can be attributed to variation in series and shunt resistance of the device affected by improper connection between subsequent layers due to shaking or bending of the device while handing and making measurements etc. The J_{SC} of the devices remains almost similar in this period of time which might be due to a sort of balance between improvement due to the morphology of the photoactive layer and degradation due to poor connection that leads to improved charge carrier generation/transportation and poor charge collection respectively [37–40]. As a result, these devices, even in this unencapsulated state, managed to retain around 80% of their initial PCE for ~500 h under ambient conditions, as shown in Fig. 9. Here T₈₀ corresponds to the time in which the PCE of the fabricated device reduced to 80% of its initial value. These findings shed light on the complex interplay between the intrinsic properties of the perovskite material and the external factors that impact the stability of PvSCs. While further advancements are necessary to enhance stability and mitigate performance degradation, the observed retention of PCE under ambient conditions and bending stress serves as a steppingstone toward the future development of durable and commercially viable PvSCs.

Further, to evaluate the stability of the devices when subjected to mechanical bending, we assessed their performance after bending them to a radius of ~5 mm (Fig. 10). It is worth noting that after 50 bending cycles, the PCE of the device experienced a reduction, however, it still retains ~60% of its initial PCE. The decrease in the performance is

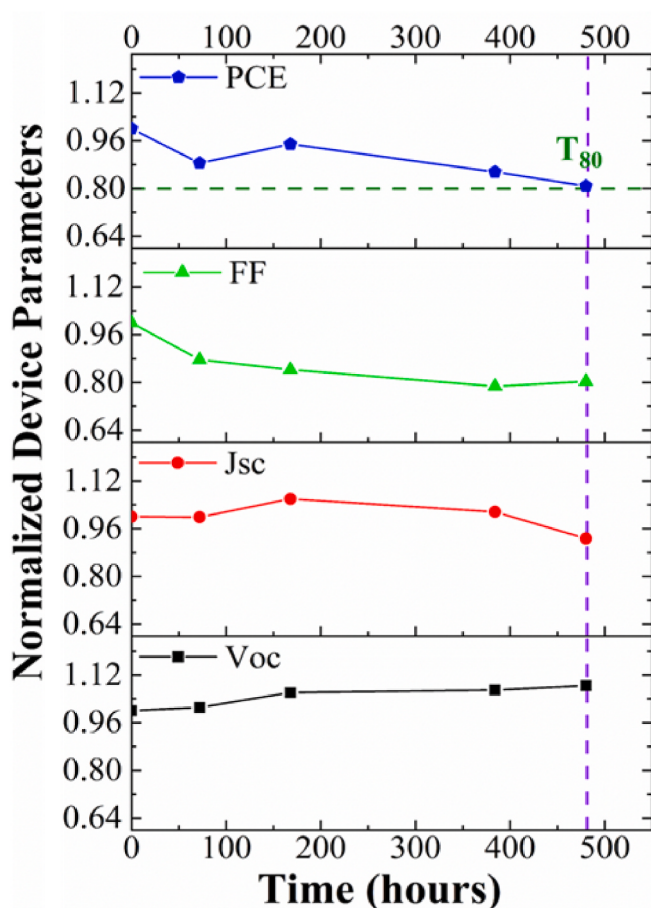


Fig. 9. Variation of electrical parameters of the best-performing device over a period of 500 h. The dashed vertical line (purple) is representing different device parameters corresponding to T_{80} of the device.

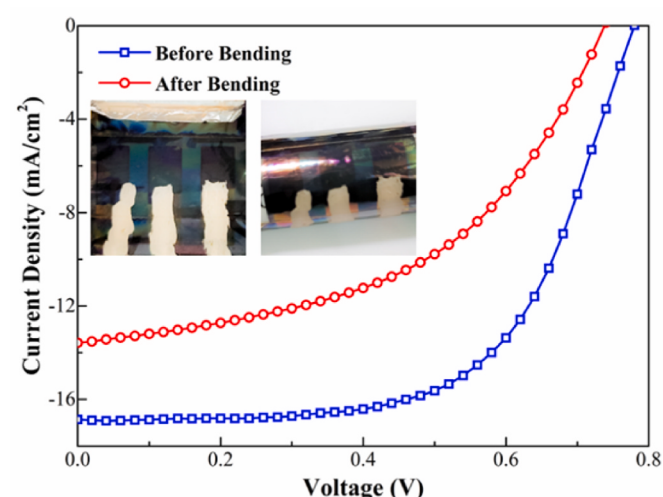


Fig. 10. Variation in JV characteristics of the device before and after 50 bending cycles at a radius of ~ 5 mm. **Inset:** Images of straight and bent devices.

believed to occur because of several reasons, including the mechanical stress developed in different layers of the device. The stress in the photoactive layer leads to increase in charge recombination inside this layer because of crack formation and grain disintegration of the perovskite film [41,42]. Secondly, it has been observed that the ultrathin metal film based TEs also suffer from minor increased sheet resistance

when bent resulting into poor charge collection and hence a lower device performance [23,43]. Also, it needs to be noted that the continuous bending at such a low radius of curvature leads to poor interfacial connections between carrier transport and photoactive layer resulting into performance degradation [44]. Additionally, it is crucial to observe that the bending analysis was conducted at an extremely acute ~ 5 mm radius of curvature, representing a sharp bend. Given that real-time applications often involve varying radii of curvature, ranging from several centimeters to over a meter, the device performance is anticipated to remain consistent across this bending range. While this reduction in efficiency signals a sensitivity to mechanical strain, the fact that the device retained a substantial portion of its performance demonstrates a promising level of stability. These findings shed light on the complex interplay between the intrinsic properties of the perovskite material and the external factors that impact the stability of PvSCs. While further advancements are necessary to enhance stability and mitigate performance degradation, the observed retention of PCE under ambient conditions and bending stress serves as a stepping stone toward the future development of durable and commercially viable PvSCs.

4. Conclusion

In conclusion, this work highlights the utilization of kitchen-grade aluminium foil as a lightweight and cost-effective substrate-cum-electrode for the fabrication of flexible photovoltaic devices. By overcoming the limitations of polymer substrates and incorporating an indium-free, oxide-metal-oxide (OMO) based transparent electrode, impressive results were achieved. The fabricated devices demonstrated a PCE of over 10.64% and a high specific power of over 3.5 W/g, surpassing the performance of conventional solar cells. This work also includes a comprehensive bending analysis to assess the mechanical stability of the fabricated devices by subjecting the devices to bending with a radius of 5 mm. Furthermore, the scalability of the fabricated devices was demonstrated by fabricating a large-area device, showcasing the potential for upscaling the production process. These advancements contribute to the practicality and viability of the presented flexible photovoltaic devices for real-world applications. These findings open up new possibilities for the development of lightweight and flexible photovoltaic devices, offering potential applications in wearable and portable electronics. By addressing the challenges associated with polymer substrates and exploring alternative materials and fabrication techniques, this study contributes to the advancement of flexible photovoltaic technologies. The use of metallic foil as a substrate-cum-electrode provides a practical and efficient approach to the realization of lightweight and mechanically robust devices. Overall, this research offers valuable insights into the fabrication of flexible photovoltaic devices and lays the foundation for further advancements in the field of renewable energy and portable electronics.

CRediT authorship contribution statement

Arun Kumar: Writing – original draft, Visualization, Software, Methodology, Conceptualization. **Sonia Rani:** Software, Methodology. **Dhriti Sundar Ghosh:** Writing – review & editing, Supervision, Resources, Funding acquisition.

Declaration of competing interest

The authors declare that they have no known competing financial interests or personal relationships that could have appeared to influence the work reported in this paper.

Data availability

Data will be made available on request.

Acknowledgement

DSG acknowledges funding support from the Department of Science and Technology (DST) & Science and Engineering Research Board (SERB) of India via grant CRG/2022/004055. AK and SR acknowledge Prime Minister Research Fellowship (PMRF-192002-1086 and PMRF-192002-2025 respectively).

Appendix A. Supplementary data

Supplementary data to this article can be found online at <https://doi.org/10.1016/j.solmat.2024.112737>.

References

- [1] M. Kaltenbrunner, G. Adam, E.D. Glowiak, M. Drack, R. Schwödauer, L. Leonat, D.H. Apaydin, H. Groiss, M.C. Scharber, M.S. White, N.S. Sariciftci, S. Bauer, Flexible high power-per-weight perovskite solar cells with chromium oxide-metal contacts for improved stability in air, *Nat. Mater.* 14 (2015) 1032–1039, <https://doi.org/10.1038/nmat4388>.
- [2] J. Yoon, H. Sung, G. Lee, W. Cho, N. Ahn, H.S. Jung, M. Choi, Superflexible, high-efficiency perovskite solar cells utilizing graphene electrodes: towards future foldable power sources, *Energy Environ. Sci.* 10 (2017) 337–345, <https://doi.org/10.1039/c6ee02650h>.
- [3] H. Xie, X. Yin, Y. Guo, J. Liu, W. Que, G. Wang, Recent progress of flexible perovskite solar cells, *Phys. Status Solidi Rapid Res. Lett.* 13 (2019) 1–23, <https://doi.org/10.1002/pssr.201800566>.
- [4] P. Holzhey, M. Prettl, S. Collavini, N.L. Chang, M. Saliba, Toward commercialization with lightweight, flexible perovskite solar cells for residential photovoltaics, *Joule* 7 (2023) 257–271, <https://doi.org/10.1016/j.joule.2022.12.012>.
- [5] National Renewable Energy Laboratory, (n.d.). <https://www.nrel.gov/pv/cell-efficency.html> (accessed September 10, 2023).
- [6] M.A. Green, A. Ho-Baillie, H.J. Snaith, The emergence of perovskite solar cells, *Nat. Photonics* 8 (2014) 506–514, <https://doi.org/10.1038/nphoton.2014.134>.
- [7] T. Grossêtéte, A. Rivaton, J.L. Gardette, C.E. Hoyle, M. Ziemer, D.R. Fagerburg, H. Clauberger, Photochemical degradation of poly(ethylene terephthalate)-modified copolymer, *Polymer (Guildf)* 41 (2000) 3541–3554, [https://doi.org/10.1016/S0032-3861\(99\)00580-7](https://doi.org/10.1016/S0032-3861(99)00580-7).
- [8] L.G. Molokanova, Y.K. Kochnev, A.N. Nechaev, S.N. Chukova, P.Y. Apel, Effect of ultraviolet radiation on polyethylene naphthalate films irradiated with high-energy heavy ions, *High Energy Chem.* 51 (2017) 182–188, <https://doi.org/10.1134/S0018143917030109>.
- [9] M. Wang, Y. Feng, Q. Dong, J. Bian, C. Ma, R. Chen, Y. Shi, Degradation mechanism of flexible perovskite solar cells: investigated by tracking of the heterojunction property, *Mater. Res. Bull.* 123 (2020) 110696, <https://doi.org/10.1016/j.materresbull.2019.110696>.
- [10] P. Subudhi, D. Punetha, Progress, challenges, and perspectives on polymer substrates for emerging flexible solar cells: a holistic panoramic review, *Prog. Photovoltaics Res. Appl.* 31 (2023) 753–789, <https://doi.org/10.1002/pip.3703>.
- [11] D.S. Ghosh, K. Leo, Microcavity-enhanced semitransparent electrodes for oligothiophene small-molecule organic solar cells, *Adv. Electron. Mater.* 3 (2017), <https://doi.org/10.1002/aeml.201600518>.
- [12] A. Kumar, S. Rani, D. Sundar Ghosh, Thermally stable indium-free transparent electrode using ultrathin Ag film, *Mater. Today Proc.* (2022), <https://doi.org/10.1016/j.matpr.2022.06.312>.
- [13] N. Ahn, D.Y. Son, I.H. Jang, S.M. Kang, M. Choi, N.G. Park, Highly reproducible perovskite solar cells with average efficiency of 18.3% and best efficiency of 19.7% fabricated via Lewis base adduct of lead(II) iodide, *J. Am. Chem. Soc.* 137 (2015) 8696–8699, <https://doi.org/10.1021/jacs.5b04930>.
- [14] A. Kumar, S. Rani, N.K. Rana, M.R. Samantaray, N. Chander, D.S. Ghosh, Thermally oxidized ultrathin copper film as low-cost hole-transport layer in planar perovskite solar cells, *Sol. Energy* 244 (2022) 457–464, <https://doi.org/10.1016/j.solener.2022.08.067>.
- [15] M. Saliba, J.P. Correa-Baena, C.M. Wolff, M. Stolterfoht, N. Phung, S. Albrecht, D. Neher, A. Abate, How to make over 20% efficient perovskite solar cells in regular (n-i-p) and inverted (p-i-n) architectures, *Chem. Mater.* 30 (2018) 4193–4201, <https://doi.org/10.1021/acs.chemmater.8b00136>.
- [16] A. Kumar, S. Rani, N. Chandrarakar, D. Sundar Ghosh, High work function thermally stable OMO-based transparent electrode for optoelectronic applications, *Mater. Today Proc.* (2023), <https://doi.org/10.1016/j.matpr.2023.02.246>.
- [17] B. Abdollahi Nejand, P. Nazari, S. Gharibzadeh, V. Ahmadi, A. Moshaii, All-inorganic large-area low-cost and durable flexible perovskite solar cells using copper foil as a substrate, *Chem. Commun.* 53 (2017) 747–750, <https://doi.org/10.1039/C6CC07573H>.
- [18] H.J. Seok, H.K. Kim, Study of sputtered ITO films on flexible invar metal foils for curved perovskite solar cells, *Metals* 9 (2019), <https://doi.org/10.3390/met9020120>.
- [19] Y. Xiao, G. Han, H. Zhou, J. Wu, An efficient titanium foil based perovskite solar cell: using a titanium dioxide nanowire array anode and transparent poly(3,4-ethylenedioxythiophene) electrode, *RSC Adv.* 6 (2016) 2778–2784, <https://doi.org/10.1039/c5ra23430a>.
- [20] B.T. Feleki, R.K.M. Bouwer, V. Zardetto, M.M. Wienk, R.A.J. Janssen, p-i-n perovskite solar cells on steel substrates, *ACS Appl. Energy Mater.* 5 (2022) 6709–6715, <https://doi.org/10.1021/acsae.2c00291>.
- [21] B.T. Feleki, R.K.M. Bouwer, M.M. Wienk, R.A.J. Janssen, Perovskite solar cells on polymer-coated smooth and rough steel substrates, *Sol. RRL* 6 (2022), <https://doi.org/10.1002/solr.202100898>.
- [22] X. Wang, Z. Li, W. Xu, S.A. Kulkarni, S.K. Batabyal, S. Zhang, A. Cao, L.H. Wong, TiO₂ nanotube arrays based flexible perovskite solar cells with transparent carbon nanotube electrode, *Nano Energy* 11 (2015) 728–735, <https://doi.org/10.1016/j.nanoen.2014.11.042>.
- [23] N. Formica, P. Mantilla-Perez, D.S. Ghosh, D. Janner, T.L. Chen, M. Huang, S. Garner, J. Martorell, V. Pruneri, An indium tin oxide-free polymer solar cell on flexible glass, *ACS Appl. Mater. Interfaces* 7 (2015) 4541–4548, <https://doi.org/10.1021/am5071909>.
- [24] P. Holzhey, M. Prettl, S. Collavini, C. Mortan, M. Saliba, Understanding the impact of surface roughness: changing from FTO to ITO to PEN/ITO for flexible perovskite solar cells, *Sci. Rep.* 13 (2023) 6375, <https://doi.org/10.1038/s41598-023-33147-6>.
- [25] S. Rani, A. Kumar, D.S. Ghosh, Oxide–metal–oxide based transparent electrodes and their potential application in semitransparent perovskite solar cells-optical modeling studies, *Sol. RRL* n/a (2023) 2200863, <https://doi.org/10.1002/solr.202200863>.
- [26] S. Jung, K.Y. Kim, Y. Il Lee, J.H. Youn, H.T. Moon, J. Jang, J. Kim, Optical modeling and analysis of organic solar cells with coherent multilayers and incoherent glass substrate using generalized transfer matrix method, *Jpn. J. Appl. Phys.* 50 (2011), <https://doi.org/10.1143/JJAP.50.122301>.
- [27] G.S. Han, S. Lee, M.L. Duff, F. Qin, J.K. Lee, Highly bendable flexible perovskite solar cells on a nanoscale surface oxide layer of titanium metal plates, *ACS Appl. Mater. Interfaces* 10 (2018) 4697–4704, <https://doi.org/10.1021/acsm.7b16499>.
- [28] J. Jaiswal, S. Mourya, G. Malik, S. Chauhan, R. Daipuriya, M. Singh, R. Chandra, Enhanced optical absorption of Ti thin film: coupled effect of deposition and post-deposition temperatures, *JOM* 69 (2017) 2383–2389, <https://doi.org/10.1007/s11837-017-2546-9>.
- [29] J.-Y. Zhang, I.W. Boyd, B.J. O’Sullivan, P.K. Hurley, P. V Kelly, J.-P. Séneur, Nanocrystalline TiO₂ films studied by optical, XRD and FTIR spectroscopy, *J. Non-Cryst. Solids* 303 (2002) 134–138, [https://doi.org/10.1016/S0022-3093\(02\)00973-0](https://doi.org/10.1016/S0022-3093(02)00973-0).
- [30] Y. Yalcinkaya, I.M. Hermes, T. Seewald, K. Amann-Winkel, L. Veith, L. Schmid-Mende, S.A.L. Weber, Chemical strain engineering of MAPbI₃ perovskite films, *Adv. Energy Mater.* 12 (2022) 2202442, <https://doi.org/10.1002/aenm.202202442>.
- [31] Q. An, F. Paulus, D. Becker-Koch, C. Cho, Q. Sun, A. Weu, S. Bitton, N. Tessler, Y. Vaynzof, Small grains as recombination hot spots in perovskite solar cells, *Matter* 4 (2021) 1683–1701, <https://doi.org/10.1016/j.matt.2021.02.020>.
- [32] D. Kim, K. Higgins, M. Ahmadi, Navigating grain boundaries in perovskite solar cells, *Matter* 4 (2021) 1442–1445, <https://doi.org/10.1016/j.matt.2021.04.006>.
- [33] M. Nukunudompanich, G. Buduitama, K. Suzuki, K. Hasegawa, M. Ihara, Dominant effect of the grain size of the MAPbI₃ perovskite controlled by the surface roughness of TiO₂ on the performance of perovskite solar cells, *CrystEngComm* 22 (2020) 2718–2727, <https://doi.org/10.1039/DCE00169D>.
- [34] S. Rani, A. Kumar, D. Sundar Ghosh, High performance of NiO-Ag-NiO based semi-transparent perovskite solar cell, *Mater. Today Proc.* (2022), <https://doi.org/10.1016/j.matpr.2022.06.211>.
- [35] X. Rong, H. Tian, W. Bi, H. Jin, T. Zhang, D. Guo, K. Zhao, Impact of metal electrode work function of CH₃NH₃PbI₃/p-Si planar heterojunction perovskite solar cells, *Sol. Energy* 158 (2017) 424–431, <https://doi.org/10.1016/j.solener.2017.08.050>.
- [36] M.R. Samantaray, N.K. Rana, A. Kumar, D.S. Ghosh, N. Chander, Stability study of large-area perovskite solar cells fabricated with copper as low-cost metal contact, *Int. J. Energy Res.* 46 (2022) 1250–1262, <https://doi.org/10.1002/er.7243>.
- [37] K. Takahashi, Y. Suzuki, Perovskite solar cells with CuI inorganic hole conductor, *Jpn. J. Appl. Phys.* 56 (2017) 08MC04, <https://doi.org/10.7567/jjap.56.08mc04>.
- [38] F. Matteocci, L. Cinà, E. Lamanna, S. Cacovich, G. Divitini, P.A. Midgley, C. Ducati, A. Di Carlo, Encapsulation for long-term stability enhancement of perovskite solar cells, *Nano Energy* 30 (2016) 162–172, <https://doi.org/10.1016/j.nanoen.2016.09.041>.
- [39] T.T. Ngo, E.M. Berea, R. Tena-Zaera, I. Mora-Seró, Spray-pyrolyzed ZnO as electron selective contact for long-term stable planar CH₃NH₃PbI₃ perovskite solar cells, *ACS Appl. Energy Mater.* 1 (2018) 4057–4064, <https://doi.org/10.1021/acsaem.8b00733>.
- [40] S. Moghadamzadeh, I.M. Hossain, M. Jakoby, B. Abdollahi Nejand, D. Rueda-Delgado, J.A. Schwenzer, S. Gharibzadeh, T. Abzieher, M.R. Khan, A. Haghhighirad, I.A. Howard, B.S. Richards, U. Lemmer, U.W. Paetzold, Spontaneous enhancement of the stable power conversion efficiency in perovskite solar cells, *J. Mater. Chem. A* 8 (2020) 670–682, <https://doi.org/10.1039/C9TA09584E>.
- [41] H. Liang, W. Yang, J. Xia, H. Gu, X. Meng, G. Yang, Y. Fu, B. Wang, H. Cai, Y. Chen, S. Yang, C. Liang, Strain effects on flexible perovskite solar cells, *Adv. Sci.* 10 (2023) 2304733, <https://doi.org/10.1002/advs.202304733>.

- [42] G. Tang, F. Yan, Recent progress of flexible perovskite solar cells, *Nano Today* 39 (2021) 101155, <https://doi.org/10.1016/j.nantod.2021.101155>.
- [43] D.S. Ghosh, Q. Liu, P. Mantilla-Perez, T.L. Chen, V. Mkhitaryan, M. Huang, S. Garner, J. Martorell, V. Pruneri, Highly flexible transparent electrodes containing ultrathin silver for efficient polymer solar cells, *Adv. Funct. Mater.* 25 (2015) 7309–7316, <https://doi.org/10.1002/adfm.201503739>.
- [44] J. Byeon, J. Kim, J.-Y. Kim, G. Lee, K. Bang, N. Ahn, M. Choi, Charge transport layer-dependent electronic band bending in perovskite solar cells and its correlation to light-induced device degradation, *ACS Energy Lett.* 5 (2020) 2580–2589, <https://doi.org/10.1021/acsenrgylett.0c01022>.